Preparation and Barrier Properties of Nanocellulose / Layered Double Hydroxide Composite Film

Mengmeng Wang, Hailong Li, Chao Du, Yun Liang, and Mengru Liu *

Cellulose nanofibrils (CNFs) were oxidized by the TEMPO oxidation system from bleached kraft eucalyptus pulp, and layered double hydroxides (LDHs) were prepared *via* the hydrothermal method. MgAl-CO_3-LDHs/CNFs composite films with different LDH ratios were prepared *via* a filtering/evaporation technique that endowed the nanocomposites with barrier and strengthening properties. The MgAl-CO_3-LDHs could uniformly disperse in the CNFs matrix with an improved reciprocal adhesion, and the surface result was smooth and continuous. The basic structure of the membrane did not change, but the thermodynamic properties and the water vapor barrier property improved. This composite membrane can be widely used in food, pharmaceutical, and chemical packaging industries as a gas-liquid barrier material.

Keywords: Nanocellulose; Layered Double Hydroxides; Composite Film; Barrier Properties

*Contact information: State Key Laboratory of Pulp and Paper Engineering, South China University of Technology, 510640, Guangzhou, China; *Corresponding author: lmr@scut.edu.cn*

INTRODUCTION

Cellulose nanofibrils (CNFs) film was peeled off from CNFs water suspension. This type of film exhibits environmental friendliness, high transparency, high mechanical performance, and enhanced gas barrier properties. With these multifunctional combinations, these nanocomposites have wide application prospects in the encapsulation of drugs, tissue engineering, or outdoor load-bearing applications. The transparency of the CNFs film was achieved by air-drying, which simultaneously improved the tensile strength and oxygen barrier properties. Because hydrogen bonding in cellulosic nanoparticles forms a dense percolating network, and the penetration of molecules is difficult in the crystalline domains of cellulose microfibrils, these composite films have been suggested for use as barrier films (Fukuzumi 2009; Belbekhouche *et al.* 2011). Due to the high hydrophilicity of nanocellulose, the fiber network of CNFs membrane material is loose, and the mechanical properties decrease when wet (Lavoine *et al*. 2012). To improve the barrier properties of CNFs based film materials, chemically modified CNFs were used, and lamellar substances were also added to extend the path of small molecules in the CNFs infiltration. Talc platelets (Liimatainen *et al.* 2013) and montmorillonite platelets (Wu *et al.* 2012) were used to increase gas barrier properties of the CNFs film. Compared with other typical platelet-like inorganic materials, the aspect ratio of layered double hydroxides (LDHs) nanosheets can be easily adjusted during the synthesis process. As an important nanoscale material, LDHs have a hydrophobic nature and layered structures, which make the movement of gas and water molecules become complex and difficult. LDHs improve the gas barrier properties of CNF films, as illustrated in Fig. 1 (Qian *et al.* 2015).

LDHs were prepared *via* a hydrothermal method, and CNFs were prepared by TEMPO oxidation / homogenization (Saito *et al.* 2007). The MgAl-CO_3-LDHs were

incorporated into the CNFs *via* a filtering/evaporation technique, which strengthened the nanocomposites. The MgAl-CO_3-LDHs dispersed uniformly into the CNFs matrix with an improved reciprocal adhesion. With the addition of LDHs, the tensile strength and water vapour permission were all improved.

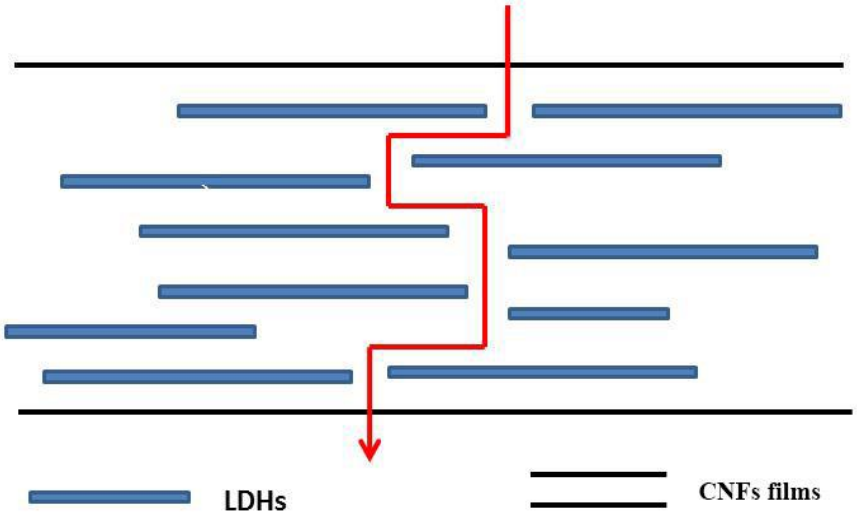

Fig. 1. The sketch map of gas permeation

EXPERIMENTAL

Materials

Bagasse bleached kraft pulp (88.34% cellulose, 8.94% hemicellulose, and 1.03% lignin) was obtained from Paper Co. Ltd., Guangzhou, China. TEMPO (2,2,6,6-tetramethylpiperidinyloxy) was purchased from Aladdin Chemistry Co., Ltd., Shanghai, China. All other chemicals used in this study were of analytical grade and purchased from the Guangzhou Chemical Reagent Factory (Guangzhou, China). Deionized water was used for all experiments.

Methods

Bleached bagasse kraft pulp (5 g) with NaBr (sodium bromide) (0.5 g), TEMPO (0.075 g), and NaClO (sodium hypochlorite) (30 mmol) was dispersed in 500 mL of deionized water at 25 °C. The mixture was stirred at pH 9.5 ± 0.3 by addition of 0.5 M of NaOH (sodium hydroxide) solution until no further decrease in pH was observed. TEMPO-oxidized cellulose fibers were obtained by thorough washing with water. The CNFs were suspended in water and homogenized by a high-pressure homogenizer.

$Mg(NO_3)_2 \cdot 6H_2O$ (0.1 mol), $Al(NO_3)_3 \cdot 9H_2O$ (0.05 mol), and urea (0.5 mol) were dispersed in 400 mL of water and then incubated in an oil bath at 110 °C for 24 h. The resulting slurry was filtered, washed thoroughly, and dried to obtain MgAl-CO_3-LDHs.

A desired amount of 0.7 wt.% CNFs water suspension was slowly added to the 0.84 wt.% MgAl-CO_3-LDHs water dispersion according to different proportions. The mixed dispersion was magnetically stirred for 24 h, and the obtained suspension was vacuum filtered to form a hydrogel. After being magnetically stirred and air-dried, a freestanding film was peeled off.

Characterizations

Scanning electron microscopy (SEM) images were collected on a Zeiss Merline microscope (Jena, Germany) at 10 kV. Fourier transform infrared (FTIR) spectra were collected on a VerTex70 spectrometer (Bruker Corp., Germany). Spectra were in the range of 400 to 4000 cm^{-1}. Diffraction patterns were obtained using a diffractometer (D8 Advance, Bruker AXS, Germany) with Cu Kα radiation (k = 0.154 nm) at 40 kV and 40 mA in the 2θ range of 5° to 60° at a speed of 1°/min. Thermogravimetric analysis (TGA) was measured on a TA Instrument Q500/Q50 System (New Castle, DE, USA) using nitrogen as the purge gas at a flow rate of 25 mL/min. Composite samples of 10 mg were heated from 30 to 600 °C at a rate of 10 °C/min. The tensile mechanical properties of the composites were measured by using a universal material testing machine (Instron 5565, Waltham, MA, USA), with a 100 N load cells. The tested samples were cut into a 40 mm × 10 mm rectangular shape, and the samples were stretched at a speed of 10 $mm \cdot min^{-1}$. Tensile properties reported here represent mean values of at least six samples' results. Water vapour permeability (WVP) of the composites was measured by weighing at 38 °C and at a relative humidity of 90%. Each sample was measured at least three times with an exposure area of 33 cm^2.

RESULTS AND DISCUSSION

SEM images of MgAl-CO_3-LDHs and the MgAl-CO_3-LDHs/CNFs composite films are shown in Fig. 2. As shown in Fig. 2(a), the SEM image of MgAl-CO_3-LDHs revealed that the samples were uniform hexagonal and about 2 μm in diameter. Figures 2(c) and 2(e) show the plan-view and sectional-view of 5 wt.% MgAl-CO_3-LDHs/CNFs films. The LDHs platelets were slightly raised on the film surface compared with the CNFs films shown in Figs. 2(b) and 2(c). LDHs dispersed well without split phase produced in CNFs matrix, and the resulting surface of the film was smooth and continuous. As shown in Figs. 2(f), 2(g), and 2(h), the interfaces become distinct with the increase of LDHs. Hence, when the content of LDHs increased from 5 wt.% to 10 wt.%, the cross section of the film was coarser, and when the LDHs content continued to increase to 15 wt.% or even 25 wt.%, the cross section of the composite film aggregated a large number of LDHs particles with obvious phase separation. This is because with the increase of LDHs contents, the LDHs agglomerated in the CNFs, and then gradually formed intercalation or aggregation structure, which resulted in the increase of membrane space and phase separation (Oliveira *et al.* 2015).

The FTIR spectra of CNF, MgAl-CO_3-LDHs, and MgAl-CO_3-LDHs/CNFs were aligned, and they are compared in Fig. 3. Compared with CNF spectra, the FTIR spectra of composite films with different LDHs ratios showed an absorption peak near 559 cm^{-1}, while the rest did not change much (Zhang *et al.* 2017). The absorption band located at 559 cm^{-1} is ascribed to the stretching vibration of metal and oxygen atoms in LDHs, and the absorbance increased with the increasing amount of LDHs contents in the mixed film. The FTIR spectra results showed that addition of LDHs to the CNFs membranes had no effect on the basic structure of the membranes, that is, the binding between LDHs and CNF was physical in nature.

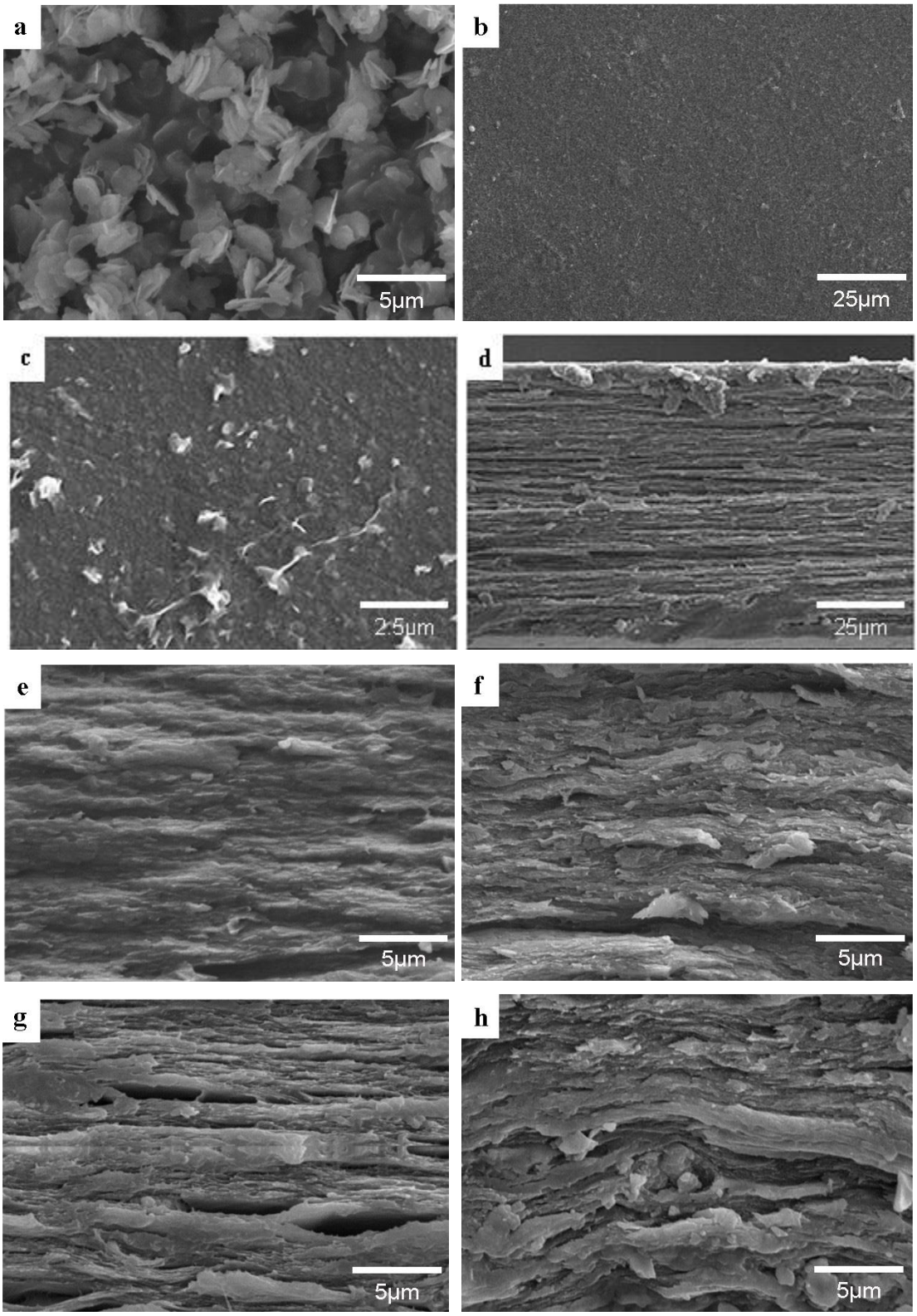

Fig. 2. SEM image of MgAl-CO_3-LDHs (a); plan-view (b) and sectional-view (d); SEM images of CNFs films, plan-view(c) and sectional-view(e); SEM images of 5 wt.% MgAl-CO_3-LDHs/CNFs composite films, sectional-view; SEM images of 10 wt.% (f), 15 wt.% (g), and 25 wt.% (h) MgAl-CO_3-LDHs/CNFs composite films

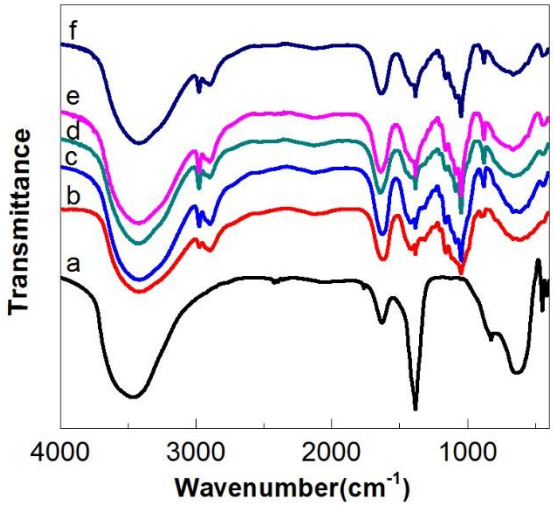

Fig. 3. FTIR spectra of CNF (a), MgAl-CO_3-LDHs (b) and 5 wt.% (c), 10 wt.% (d), 15 wt.% (e), 25 wt.% (f) MgAl-CO_3-LDHs/CNFs composite films

XRD patterns of CNF, MgAl-CO_3-LDHs, and MgAl-CO_3-LDHs/CNFs composite films are shown together in Fig. 4. As shown in Fig. 4(a), highly crystalline and monodisperse MgAl-CO_3-LDHs were prepared. From the XRD patterns of the mixed films fabricated with different LDHs loadings, the intrinsic layered symmetry of MgAl-CO_3-LDHs in the hybrid films was still retained (Hivechi and Bahrami 2016). Meanwhile, the peak intensity increased with increasing LDH loading. This showed that in the composite films, LDHs still exist as a completely layered sheet structure.

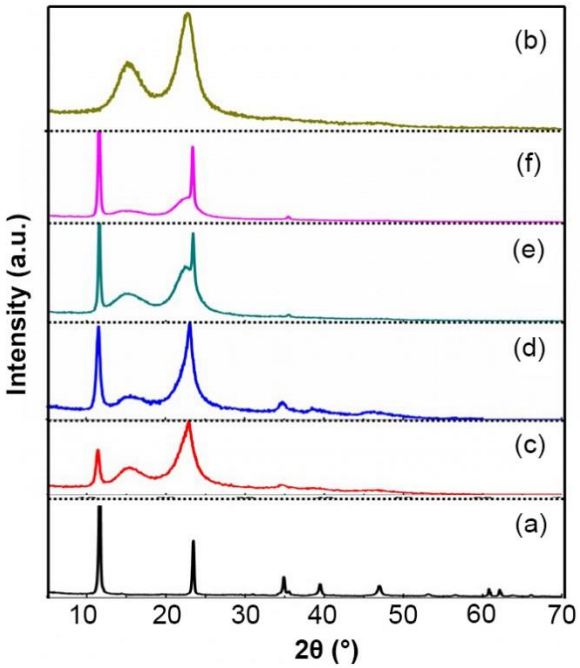

Fig. 4. XRD patterns of CNF(a), MgAl-CO_3-LDHs(b) and 5 wt.%(c), 10 wt.% (d), 15 wt.% (e), 25 wt.% (f) MgAl-CO_3-LDHs/CNFs composite films

The TGA curves of pure LDHs, CNFs, and LDHs/CNF films with various LDHs loadings are shown in Fig. 5. For pure LDHs, the temperature for removal of interlayer water molecules was from 50 to 230 °C, assigning to the first stage of weight loss. The second stage of weight loss was from 230 to 340 °C, which is ascribed to the removal of aluminum hydroxy and intercalated CO_3^{2-}. The third stage of weight loss was from 340 to 600 °C and occurs due to the loss of dehydroxylation of the interlayer magnesium metal and CO_3^{2-} (Costa *et al.* 2008). For pure CNFs films, the weight loss mainly occurred in the temperature range of 50 to 400 °C, and the residue was merely about 30%. The first stage of CNFs degradation was mainly to eliminate water. Subsequently, a large production of volatiles accompanied by the random scission of cellulose molecular chains degraded, which led to a 70% weight loss of CNFs before reaching 400 °C. The final stage of weight loss from 400 to 600 °C was the graphitization stage of cellulose, in which the residual part of the cellulose structure undergoes aromatization cyclization, and the graphite structure is gradually formed (Habibi *et al.* 2006). The TGA curves of the LDHs/CNFs films showed three stages of weight loss very similar to the pure CNFs films. The decomposition temperature of the sample gradually moved to a higher temperature, from 230 to 275 °C. All of the LDHs/CNFs films had higher decomposition rates and lower residues than the pure CNFs film; this was due to the removal of intercalated hydroxy and CO_3^{2-} as well as the dispersion of LDHs in the CNFs membrane, enhancing heat transfer (Gao *et al.* 2014). When the content of LDHs increased to 25%, the TGA curve of the composite films was similar to other composite films from 150 to 600 °C , but the DTG curve appeared two peaks around 50 °C and 110 °C. In the dehydration stage of the composite membrane, corresponding to the desorption of cellulose and the removal of water between LDHs layers, the latter plays the more important role. Therefore, appropriate contents of inorganic LDHs and CNFs in the film are necessary, and stronger interfacial interactions were produced (Shu *et al.* 2014).

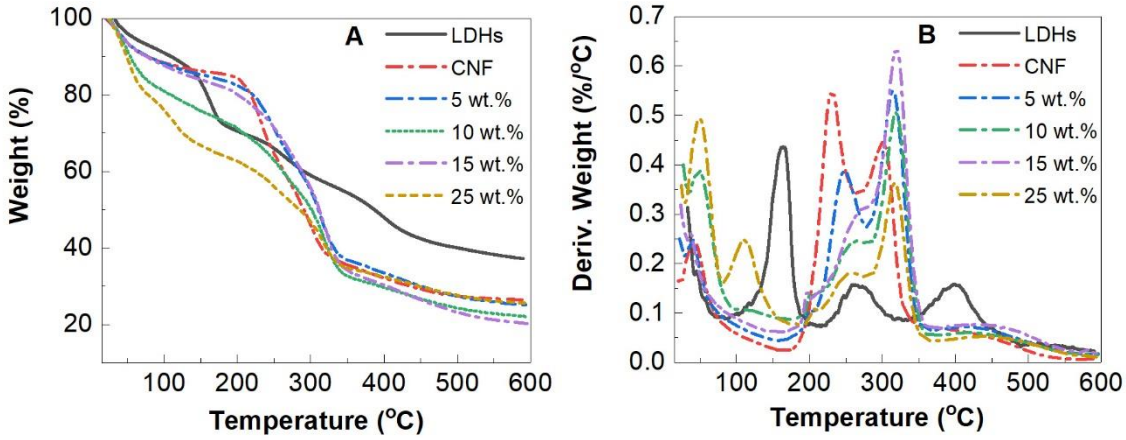

Fig. 5. TGA (A) and DTG (B) curves of CNFs/MgAl-CO_3-LDHs composite films

Representative mechanical properties and tensile curves of pure CNFs and LDHs/CNFs films are shown in Table 1 and Fig. 6. Compared with pure CNFs, the mechanical properties of the LDHs/CNFs films were significantly changed. Upon the mixing of low contents inorganic LDHs platelets in the CNFs matrix, the mechanical properties of the resulting LDHs/CNFs complex films were obviously enhanced with the increase of LDHs contents.

Table. 1. Mechanical Properties of CNFs/MgAl-CO_3-LDHs Composite Films

Content of LDHs (wt.%)	Thickness (μm)	Tensile Strength (MPa)	Elastic Modulus (MPa)	Tensile Strain (%)
0	75	73 ± 9	3008 ± 75	0.22 ± 0.03
5	80	101 ± 6	3458 ± 70	0.26 ± 0.03
10	83	84 ± 8	3581 ± 80	0.24 ± 0.04
15	87	81 ±7	2690 ± 65	0.22 ± 0.02
25	91	44 ± 8	2100 ± 90	0.22 ± 0.04

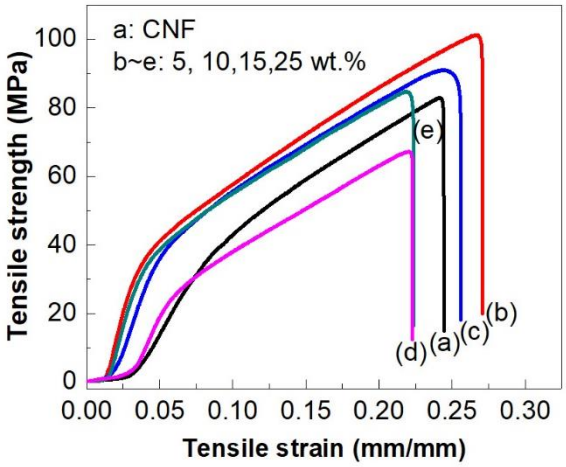

Fig. 6. Tensile strain-strength curves of CNFs/MgAl-CO_3-LDHs composite films

When the contents of LDHs increased to 5 wt.%, the tensile strength increased from 73 to 101 MPa and the elastic modulus increased from 3008 to 3458 MPa. One possible reason is that the low contents of LDHs in the composite film is easily able to form a stripping structure and disperse well so as to optimize the mechanical properties (Dou *et al.* 2014). In contrast, as the LDHs contents continued to increase to 25 wt.%, the mechanical properties of the composite film were remarkably reduced. The elastic modulus and tensile strength of the composite film reached the lowest, which were 44 MPa and 2100 MPa. Thus, the LDHs content plays an important role in the mechanical performance of LDHs/CNFs complex films. Tensile stress and elastic modulus of these films increased as the LDHs contents increased. By contrast, after reaching the maximum value, the tensile stress and modulus decreased with the further addition of LDHs. LDHs platelets are structurally similar to the structure of nano-clays, and these clay-polymer composites are more fragile than the corresponding pure polymer matrices (Sehaqui *et al.* 2013). With excess LDHs accumulated in CNFs, the gap of the composite films increased, which resulted in decreased mechanical properties of the composite films.

As shown in Fig. 7, WVP of the composite film was significantly decreased from the initial value 2332 g/m^2·24 h to 1927 g/m^2·24 h at the 10 wt.% content of LDHs. Low content of LDHs, such as 5 wt.% and 10 wt.% in the composite film, is more likely to disperse well and fill the original interstice of CNFs. This is the reason why the movement of gas and water molecules became complex. At the same time, large length-width ratios of LDHs created a tortuous path, obstructed the passage of water vapor, then hindered the

WVP. In contrast, as the LDHs content increased to 15 wt.% or even 25 wt.%, owing to the accumulation of LDHs in CNFs, the bonding was not compact, so the WVP of the composite film was markedly increased. However, all the LDHs/CNFs composite film had better WVP than pure CNFs films. From all the data above, it can be concluded that the 10 wt.% content of LDHs plays an important role in the WVP of LDHs/CNFs complex films in that the WVP of these films was remarkably reduced.

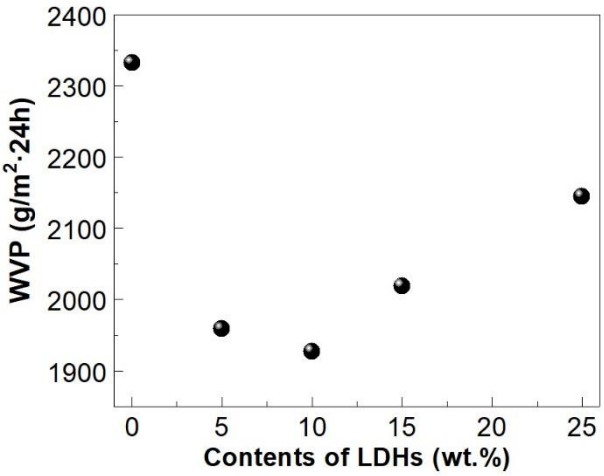

Fig. 7. Water vapor penetration of CNFs/MgAl-CO_3-LDHs composite film

CONCLUSIONS

1. The binding between layered double hydroxides (LDHs) and cellulose nanofibrils (CNF) was physical in nature. The composite films showed a high mechanical performance with the loading of LDH. When the content of MgAl-CO_3-LDHs was low (< 10 wt.%), the Young's modulus increased by 19%, the tensile strength increased by 39%, and the elasticity modulus reached 3458 MPa at the 10 wt.% LDHs/CNFs composite film. It was found to be much better than the conventional film.
2. Composite films showed enhanced gas barrier properties. When the content of MgAl-CO_3-LDHs was low (< 10 wt.%), the water vapor permeability decreased by 50% and was half of the pure CNFs film. Water vapor permeability reached 1927 g/m^2·24 h at the 10 wt.% LDHs/CNFs composite film. It was also shown to be much better than the conventional film in this respect.
3. Such enhancement in mechanical performance and barrier properties is ascribed to the strong interactions between CNFs and LDHs at the interface, where these two rigid components show strong physical adsorption. This kind of multifunctional combination renders these nanocomposites interesting for broader applications, such as the encapsulation of drugs and tissue engineering, as well as load-bearing applications outdoors. From this strategy, further development of multifunctional nanocellulose-based nanocomposites is expected.

ACKNOWLEDGMENTS

The authors acknowledge the National Key Technology Research and Development Program of the Ministry of Science and Technology of China (2015BAE02B02), the Science and Technology Planning Project of Guangdong Province (2015A020215007), the Natural Science Foundation of China (No. 31670586), the Fundamental Research Funds for the Central Universities (2017ZD091), and the State Key Laboratory of Pulp and Paper Engineering Program (2016C05) for sponsoring this research.

REFERENCES CITED

Belbekhouche, S., Bras, J., Siqueira, G., Chappey, C., Lebrun, L., Khelifi, B., Marais, S., and Dufresne, A. (2011). "Water sorption behavior and gas barrier properties of cellulose whiskers and microfibrils films," *Carbohydrate Polymers* 83(4), 1740-1748. DOI: 10.1016/j.carbpol.2010.10.036

Costa, F. R., Leuteritz, A., Wagenknecht, U., Jehnichen, D., Häußler, L., and Heinrich, G. (2008). "Intercalation of Mg-Al layered double hydroxide by anionic surfactants: Preparation and characterization," *Applied Clay Science* 38(3–4), 153-164. DOI: 10.1016/j.clay.2007.03.006

Dou, Y., Xu, S., Liu, X., Han, J., Yan, H., Wei, M., Evans, D. G., and Xue, D. (2014). "Transparent, flexible films based on layered double hydroxide/cellulose acetate with excellent oxygen barrier property," *Advanced Functional Materials* 24(4), 514-521. DOI: 10.1002/adfm.201301775

Fukuzumi, H. (2009). "Transparent and high gas barrier films of cellulose nanofibers prepared by TEMPO-mediated oxidation," *Biomacromolecules* 1(10). DOI: 10.1021/bm801065u

Gao, Y., Wu, J., Wang, Q., Wilkie, C., and O'Hare, D. (2014). "Flame retardant polymer/layered double hydroxide nanocomposites," *Journal of Materials Chemistry A* 2(29), 10996-11016. DOI: 10.1039/C4TA01030B

Habibi, Y., Chanzy, H., and Vignon, M. R. (2006). "TEMPO-mediated surface oxidation of cellulose whiskers," *Cellulose* 13(6), 679-687. DOI: 10.1007/s10570-006-9075-y

Hivechi, A., and Bahrami, S. H. (2016). "A new cellulose purification approach for higher degree of polymerization: Modeling, optimization and characterization," *Carbohydrate Polymers* 152, 280-286. DOI: 10.1016/j.carbpol.2016.07.001

Lavoine, N., Desloges, I., Dufresne, A., and Bras, J. (2012). "Microfibrillated cellulose - Its barrier properties and applications in cellulosic materials: A review," *Carbohydrate Polymers* 90(2), 735-64. DOI: 10.1016/j.carbpol.2012.05.026

Liimatainen, H., Ezekiel, N., Sliz, R., Ohenoja, K., Sirviö, J. A., Berglund, L., Hormi, O., and Niinimäki, J. (2013). "High-strength nanocellulose-talc hybrid barrier films," *ACS Applied Materials & Interfaces* 5(24), 13412. DOI: 10.1021/am4043273

Oliveira, R. L. D., Barud, H. D. S., Salvi, D. T. B. D., Perotti, G. F., Ribeiro, S. J. L., and Constantino, V. R. L. (2015). "Transparent organic-inorganic nanocomposites membranes based on carboxymethylcellulose and synthetic clay," *Industrial Crops & Products* 69, 415-423. DOI: 10.1016/j.indcrop.2015.02.015

Qian, Y., Li, S., and Chen, X. (2015). "Synthesis and characterization of LDHs using Bayer red mud and its flame-retardant properties in EVA/LDHs composites," *Journal of Material Cycles & Waste Management* 17(4), 646-654. DOI: 10.1007/s10163-015-

0409-4

Saito, T., Kimura, S., Nishiyama, Y., and Isogai, A. (2007). "Cellulose nanofibers prepared by TEMPO-mediated oxidation of native cellulose," *Biomacromolecules* 8(8), 2485. DOI: 10.1021/bm0703970

Sehaqui, H., Kochumalayil, J., Liu, A., Zimmermann, T., and Berglund, L. A. (2013). "Multifunctional nanoclay hybrids of high toughness, thermal, and barrier performances," *ACS Applied Materials & Interfaces* 5(15), 7613-7620. DOI: 10.1021/am401928d

Shu, Y., Yin, P., Liang, B., Wang, H., and Guo, L. (2014). "Bioinspired design and assembly of layered double hydroxide/poly(vinyl alcohol) film with high mechanical performance," *ACS Applied Materials & Interfaces* 6(17), 15154. DOI: 10.1021/am503273a

Wu, C. N., Saito, T., Fujisawa, S., Fukuzumi, H., and Isogai, A. (2012). "Ultrastrong and high gas-barrier nanocellulose/clay-layered composites," *Biomacromolecules* 13(6), 1927. DOI: 10.1021/bm300465d

Zhang, Q., Xu, M., Xing, L., Dang, C., Han, X., and Pu, J. W. (2017). "Enzymatic assisted ultrasonic pretreatment's effect on poplar pulp properties," *BioResources* 12(3), 6832-6843. DOI:10.15376/biores.12.3.6832-6843

Article submitted: October 21, 2017; Peer review completed: November 25, 2017; Revised version received and accepted: December 8, 2017; Published: December 12, 2017.
DOI: 10.15376/biores.13.1.1055-1064